Spectrochimica Acta Part A: Molecular and Biomolecular Spectroscopy 152 (2016) 92–100

Contents lists available at ScienceDirect

Spectrochimica Acta Part A: Molecular and Biomolecular Spectroscopy

journal homepage: www.elsevier.com/locate/saa

The molecular structure and vibrational, ^{1}H and ^{13}C NMR spectra of lidocaine hydrochloride monohydrate

Hassan M. Badawi *, Wolfgang Förner, Shaikh A. Ali

Department of Chemistry, King Fahd University of Petroleum & Minerals (KFUPM), Dhahran 31261, Saudi Arabia

HIGHLIGHTS

- The structure of lidocaine·HCl·H_2O was optimized at the DFT B3LYP level.
- The vibrational wavenumbers and NMR chemical shifts were calculated.
- Vibrational and NMR assignments were provided by combining experimental and theoretical data.

GRAPHICAL ABSTRACT

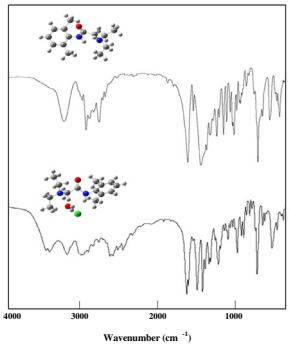

ARTICLE INFO

Article history:
Received 20 April 2015
Received in revised form 8 July 2015
Accepted 9 July 2015
Available online 10 July 2015

Keywords:
Molecular structure
Vibrational, ^{1}H and ^{13}C NMR spectra and assignments
Lidocaine hydrochloride monohydrate
Local anesthetic drug

ABSTRACT

The structure, vibrational and NMR spectra of the local anesthetic drug lidocaine hydrochloride monohydrate salt were investigated by B3LYP/6-311G** calculations. The lidocaine·HCl·H_2O salt is predicted to have the *gauche* structure as the predominant form at ambient temperature with NCCN and CNCC torsional angles of 110° and −123° as compared to 10° and −64°, respectively in the base lidocaine. The repulsive interaction between the two N–H bonds destabilized the *gauche* structure of lidocaine·HCl·H_2O salt. The analysis of the observed vibrational spectra is consistent with the presence of the lidocaine salt in only one *gauche* conformation at room temperature. The ^{1}H and ^{13}C NMR spectra of lidocaine·HCl·H_2O were interpreted by experimental and DFT calculated chemical shifts of the lidocaine salt. The RMSD between experimental and theoretical ^{1}H and ^{13}C chemical shifts for lidocaine·HCl·H_2O is 2.32 and 8.21 ppm, respectively.

1. Introduction

Lidocaine is a commonly used drug with many applications due to its antiarrhythmic and local anesthetic effects [1–8]. It mainly acts by blocking the pore-forming region of neuronal voltage-gated sodium (Na^+) channels [9]. This blockade prevents the flow of Na^+ ions across cell membranes resulting in a decrease in neuronal depolarization and the inhibition of action potential initiation and propagation [10–12]. Thus when administered for local anesthesia, lidocaine can cause reversible sensory and motor paralysis [13].

The structure of lidocaine was recently investigated at the B3LYP/6-311G** level of theory and reported to exist predominantly in a non-planar *cis* (NCCN ~0°) structure [14]. The calculated NCCN torsional angle of 9.6° and the CNCC torsional angle of −132.2° were in a good qualitative agreement with the reported X-ray angles of (3.1 and −102.67) and (13.0° and −77.9°) for two H-bonded dimers, respectively [15]. The relative intensity and broadness of the N–H stretching band in the FTIR spectrum suggest

* Corresponding author.
E-mail address: hbadawi@kfupm.edu.sa (H.M. Badawi).

http://dx.doi.org/10.1016/j.saa.2015.07.060
1386-1425/

the presence of moderate hydrogen bonding in the condensed phase of lidocaine [15].

Lidocaine base is insoluble in water and therefore for clinical use, it is generally formulated as the soluble hydrochloride salt {2-Diethylamino-*N*-(2,6-dimethylphenyl)acetamide hydrochloride monohydrate}. Administering a medication in its soluble form, especially as an injectable, is important for achieving rapid response, ease of administration, and decreased pain at site of injection. Systemically, lidocaine hydrochloride dissociates into the positively charged lidocaine which equilibrates with its neutral form. Both the charged and the neutral lidocaine play a role in its mechanism of action [16–18]. Here, we expand on our previous structural studies of lidocaine [14] to include its salt form, lidocaine hydrochloride monohydrate (lidocaine·HCl·H_2O). We assigned the vibrational and NMR spectra of the molecule on the basis of its combined experimental and computed data at the B3LYP/6-311G** level of theory. The results of the work are presented herein. For the atom numbering see Fig. 1.

2. Experimental infrared and Raman spectra

The lidocaine hydrochloride monohydrate salt (Fig. 1) was prepared [19] as shown in S1. The infrared and Raman spectra of lidocaine·HCl·H_2O (Fig. 2) and its anhydrous form lidocaine·HCl (Fig. 1) were recorded using a Nicolet 6700 FT-IR spectrometer equipped with a globar source, a KBr beamsplitter, and a DTGS KBr detector in the region 4000–400 cm^{-1}. A Nicolet NXR FT-Raman module equipped with a CaF_2 beamsplitter and an InGaAs detector was used to collect the Raman spectrum (Fig. 2) of lidocaine·HCl·H_2O. A Helium–Neon laser source operating at approximately 0.5 W was utilized for excitation of the sample.

2.1. Experimental ^1H and ^{13}C NMR spectra

The ^1H and ^{13}C NMR spectra of lidocaine·HCl·H_2O were measured on a JEOL LA 500 MHz spectrometer using $CDCl_3$ as solvent and tetramethylsilane (TMS) as internal standard, as shown in comparison with the neutral lidocaine [8] in Figs. 3 and 4. For lidocaine·HCl·H_2O: δ_H ($CDCl_3$): 1.50 (3H, t, *J* 7.3 Hz), 2.06 (2H, s, OHs), 2.25 (6H, s), 3.40 (2H, dqd, J 4.5, 7.3, 13.2 Hz), 3.54 (2H, dq, *J* 7.3, 13.2 Hz), 4.42 (2H, d, J 4.0 Hz), 7.02 (1H, d, *J* 8.3 Hz), 7.02 (1H, d, *J* 6.0 Hz), 7.06 (1H, dd, *J* 6.0, 8.6 Hz), 10.18 (1H, s, CONH), 11.07 (1H, br, NH^+) (TMS: 0.00); δ_C ($CDCl_3$): 10.00, 18.69, 49.13, 50.94, 127.48, 128.12, 133.11, 135.11, 162.93, (TMS: 0.00).

3. Computational details

The GAUSSIAN 09 program [20], running on a 128 node High performance e-1350 IBM Cluster was used to carry out the density functional B3LYP calculations with the 6-311G** basis set. The possible planar and non-planar structures of lidocaine hydrochloride monohydrate (Fig. 1) were optimized and the energies and dipole moments were predicted at the DFT level of calculation. From the calculations, the planar forms of the salt were found to turn into the non-planar structures upon completion of optimization. The optimized energies of the lidocaine salt at the B3LYP level are listed in Tables 1 and S1. Some of the optimized parameters at the B3LYP/6-311G** level of theory are shown in Table 2.

The optimized structural parameters of the low energy form of lidocaine·HCl·H_2O at the B3LYP/6-311G** level are used to compute the ^1H and ^{13}C shielding constants (σ) of the lidocaine salt and of the reference TMS by the Gauge Independent Atomic Orbital (GIAO) method [21,22] and listed in Tables 2 and 3. The chemical shifts (δ) are calculated as: ($\delta = \sigma_{TMS} - \sigma$), where, σ is σ_H or σ_C of H or C atoms (Tables S2 and S3). The estimated chemical shifts are compared to the corresponding experimental values in Table 3. Fig. S1 shows the atom numbering in the calculated high energy form of the anhydrous salt.

3.1. Vibrational frequencies and normal coordinate analysis

The optimized structural parameters of lidocaine hydrochloride monohydrate in its low energy *gauche* conformation were used to calculate its vibrational frequencies at the B3LYP/6-311G** level of theory. Also we calculated the vibrational frequencies of the protonated form, the ammonium ion without the Cl atom and the H_2O molecule for potential energy calculations. The torsional angles of the heavy atoms of the lidocaine protonated ion were kept constant and the same as those of the optimized lowest energy G1 structure of lidocaine·HCl·H_2O. Complete assignments of the normal vibrational modes were proposed on the basis of normal coordinate calculations [23] and the calculated infrared band intensities, Raman line activities, depolarization ratios, *Gauss-View* [24] and experimental infrared and Raman spectra of the lidocaine salt (Fig. 2). The complete sets of the internal and the symmetry coordinate of the protonated lidocaine are listed in Tables S4 and S5. The vibrational assignments of the normal modes are listed in Tables 4 and S6.

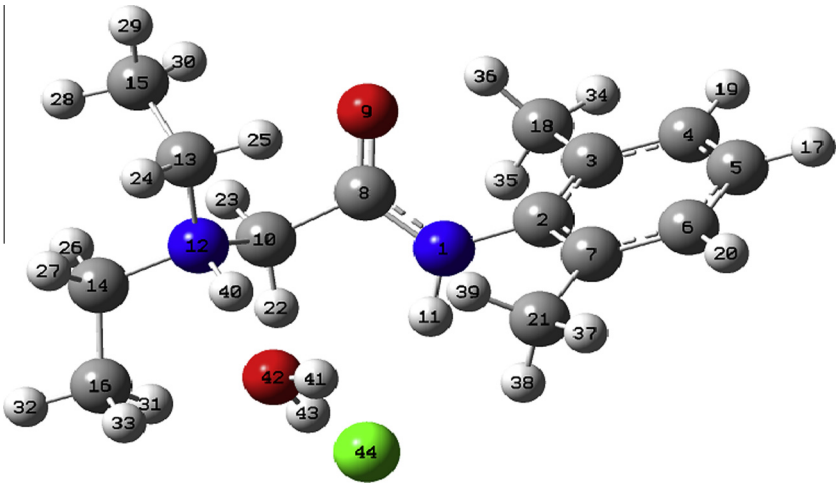

Fig. 1. Atom numbering of the optimized non-planar structures of lidocaine hydrochloride monohydydrate.

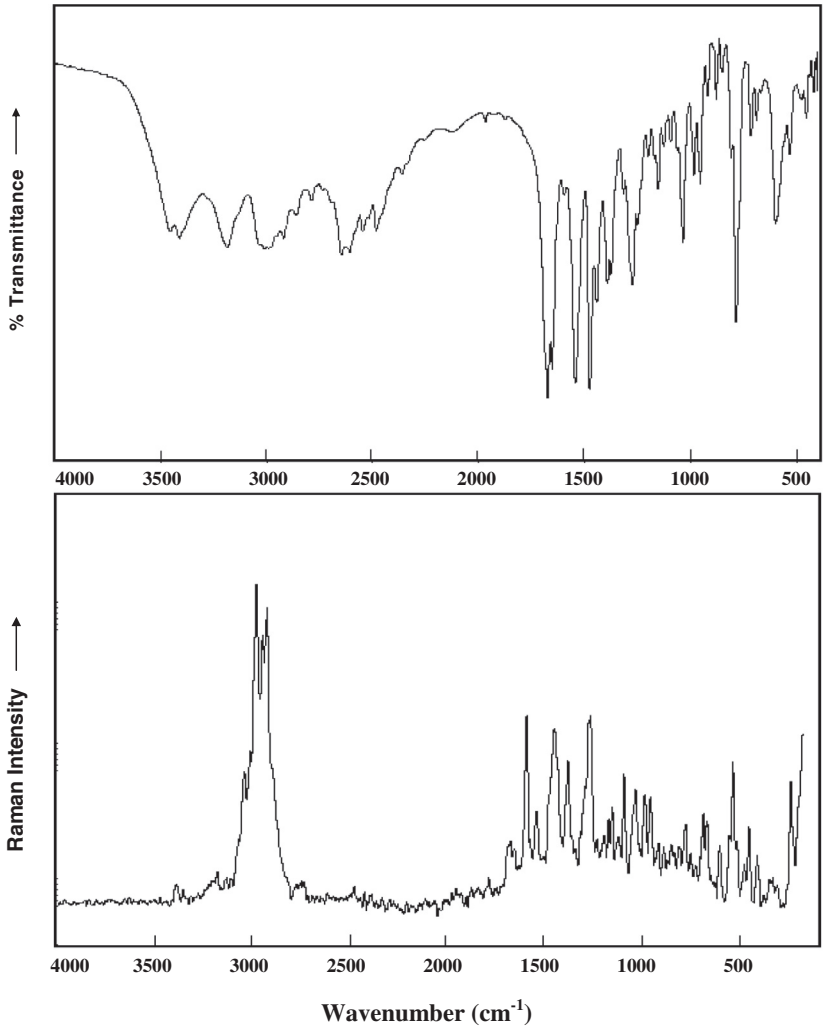

Fig. 2. Infrared (upper) and Raman (lower) spectra of lidocaine·HCl·H_2O.

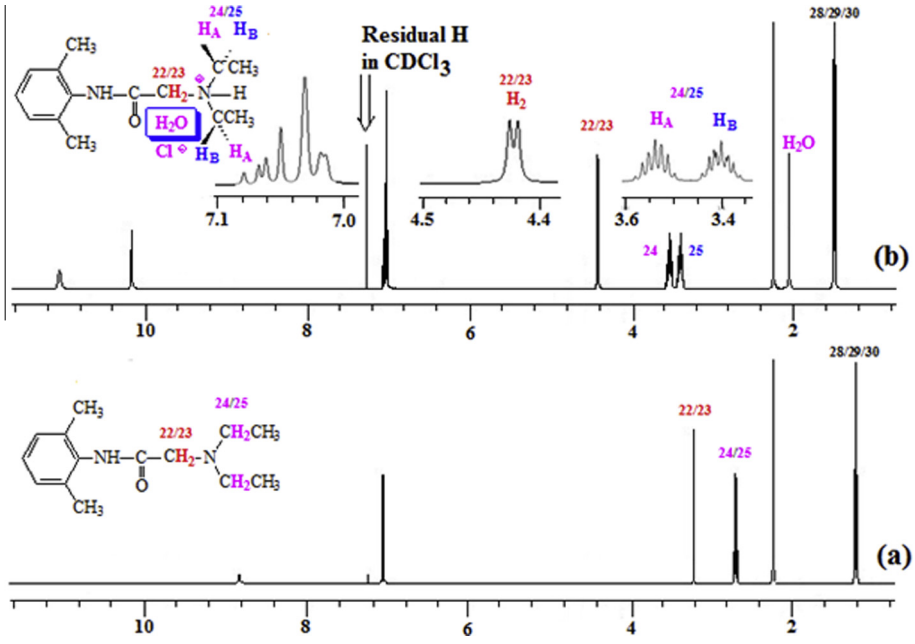

Fig. 3. The ^1H spectra of (a) lidocaine and (b) lidocaine·HCl·H_2O.

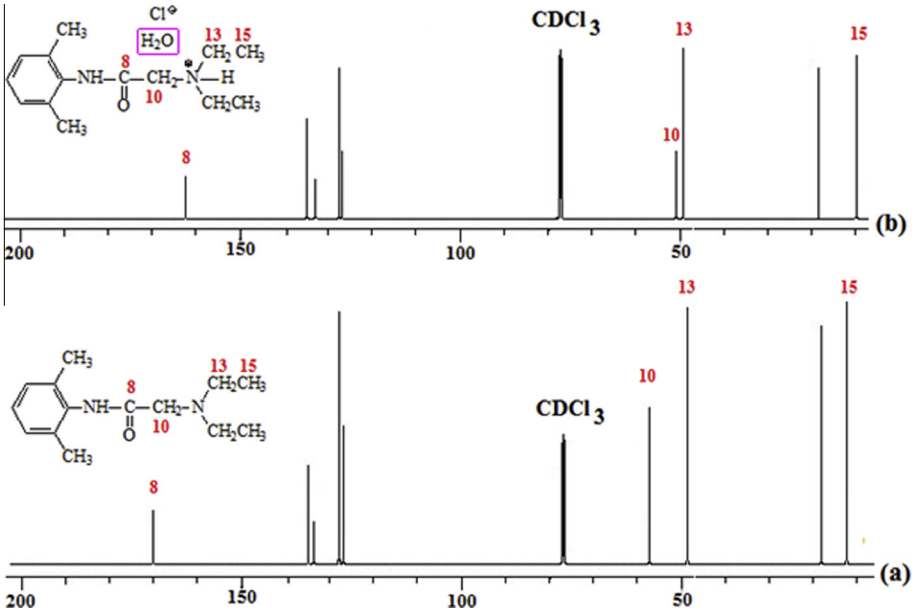

Fig. 4. The ^{13}C spectra of (a) lidocaine and (b) lidocaine·HCl·H_2O.

Table 1
Calculated relative energies *E* (kcal/mol) of the non-planar (*G*) structures of lidocaine hydrochloride monohydrate at the B3LYP/6-311G** level of calculations.

Structure	B3LYP	
	(ϕ_1, ϕ_2, ϕ_3, ϕ_4, ϕ_5, ϕ_6, ϕ_7, ϕ_8, ϕ_9)[a]	ΔE
G1	(110, −64, 0, 172, 48, 176, 63, 71, −69)	0.000
G2	(84, −60, −1, 169, 178, 48, −69, 178, −72)	1.067
G3	(127, −60, −3, 165, 76, −53, 72, −154, −166)	10.414

[a] $\phi_1 - \phi_9$ are the $N_1C_8C_{10}N_{12}$, $C_8N_1C_2C_3$, $O_9C_8N_1C_2$, $H_{11}N_1C_2O_9$, $C_{13}N_{12}C_{10}C_8$, $C_{14}N_{12}C_{10}C_8$, $C_{15}C_{13}N_{12}C_{10}$, $C_{16}C_{13}N_{12}C_{10}$ and $H_{40}N_{12}C_{10}C_8$ torsional angles, respectively (see Fig. 1).

Table 2
Selected torsional angles (degrees) of the optimized non-planar *structures* of lidocaine (LDC) and its lidocaine hydrochloride monohydrate (LDCH) salt as calculated at the B3LYP/6-311G** level of theory.

Parameters	LDC	LDCH
($N_1C_8C_{10}N_{12}$)	9.58	109.92
($O_9C_8C_{10}N_{12}$)	−171.47	−71.84
($O_9C_8C_1C_2$)	−4.88	0.01
($C_3C_2N_1C_8$)	−123.30	−64.10
($C_{10}C_8N_1C_2$)	174.00	178.12
($C_{13}N_{12}C_{10}C_8$)	−139.53	47.89
($C_{14}N_{12}C_{10}C_8$)	87.68	175.85
($C_{15}C_{13}N_{12}C_{10}$)	73.51	63.33
($C_{16}C_{13}N_{12}C_{10}$)	71.60	70.98
($H_{40}N_{12}C_{10}C_8$)		−68.85
($O_{42}H_{40}N_{12}C_{10}$)		−83.81
($Cl_{44}H_{40}N_{12}C_{10}$)		−29.46

4. Results and discussion

Lidocaine is commonly formulated as a topical gel, an intravenous or an intradermal solution, depending on the intended use. Studying the structural profile of lidocaine and its salt forms will help in optimizing the formulation and drug delivery method to achieve maximum efficacy and minimal side effects. The interesting pharmaceutical [25–29] and structural [19,30,31] properties of lidocaine hydrochloride have prompted the present study of its conformational profile and vibrational, ^1H and ^{13}C NMR spectra. The predominant structure of lidocaine hydrochloride monohydrate was characterized by X-ray crystallography as fully hydrogen bonded with adjacent cations linked by water molecules in chains. The chains are reported to be joined in pairs by chloride ions that bind NH^+ and H_2O moieties in different chains [30,31].

4.1. Molecular structures and stability

The addition of the HCl and H_2O moieties to the lidocaine molecular frame leads to significant changes in the structural stability of the low energy structure of the lidocaine salt. For example, the $N_1C_8C_{10}N_4$ torsional angle in the lidocaine·HCl·H_2O salt is calculated to be 109°, as compared to 10° in lidocaine [14] as shown in Table 2. This significant increase in the NCCN torsional angle is a result of strong repulsive interaction between the two N–H bonds in the lidocaine salt (see Fig. 1). This steric hinderance also has affected the orientation of the N-diethyl moiety about the N–C bond (see the CNCC angle in Table 2). Also, the calculated CCNC torsional angle of the phenyl ring about the N–C bond is predicted to be significantly influenced by the HCl and H_2O addition (−123° in lidocaine and −64° in the lidocaine·HCl·H_2O salt). For the terminal methyl groups of the N-diethyl moiety the CCNC torsional angle seems not to be drastically affected by the HCl and H_2O cluster in the molecular structure of the lidocaine salt (Table 2).

The stability of the optimized structure of the lidocaine salt (Fig. 1) can be explained on the basis of the hydrogen bonding in the system suggested by X-ray crystallography [30,31]. If the large chloride ion would be close to the NH^+ group, then it would block

Table 3
Observed (Exp) and calculated (Calc) (at the B3LYP/6-311G** level) ^{1}H and ^{13}C chemical shifts[b] δ (ppm) and the calculated-experimental difference (Δ) of lidocaine hydrochloride monohydrate (reference to TMS).

H atoms[a,b]	Exp	Calc	Δ[c]	C atoms[a,b]	Exp	Calc	Δ[c]
H11	10.18	11.47	1.29	C2	135.11	141.68	6.57
H17	7.06	7.18	0.12	C3	133.11	142.87	9.76
H19	7.02	7.17	0.15	C4	128.12	131.64	3.52
H20	7.02	7.12	0.10	C5	127.48	132.69	5.21
H22	4.42	5.74	1.32	C6	128.12	132.20	4.08
H23	4.42	2.60	−1.82	C7	133.11	140.83	7.72
H24	3.54	2.54	−1.00	C8	162.93	164.15	1.22
H25	3.40	3.71	0.31	C10	50.94	53.48	2.54
H26	3.54	2.79	−0.75	C13	49.13	53.89	4.76
H27	3.40	2.69	−0.71	C14	49.13	53.32	4.19
H28	1.50	0.96	−0.54	C15	10.00	7.57	−2.43
H29	1.50	0.98	−0.52	C16	10.00	12.80	2.80
H30	1.50	2.13	0.63	C18	18.69	20.77	2.08
H31	1.50	2.14	0.64	C21	18.69	22.73	4.04
H32	1.50	1.02	−0.48				
H33	1.50	2.02	0.52				
H34	2.25	1.88	−0.43				
H35	2.25	2.08	−0.17				
H36	2.25	2.60	0.35				
H37	2.25	1.80	−0.45				
H38	2.25	3.37	1.12				
H39	2.25	1.85	−0.40				
H40	11.07	10.87	−0.20				
H41	2.06	1.14	−0.92				
H43	2.06	8.42	6.36				

[a] Atoms numbering in Fig. 1.
[b] The chemical shift δ is computed as: $\delta = \sigma_{TMS} - \sigma_{sample}$; where, σ is the calculated isotropic shielding constant at the B3LYP/6-311G** level (see Tables S4 and S5).
[c] The calculated RMSD is 2.32 and 8.21 ppm for the ^{1}H and the ^{13}C chemical shifts, respectively.

access of the water molecule to the NH^+ group, and the oxygen atom in the water molecule could not form its two strong N–H···O hydrogen bonds to the hydrogen atom and also not the O–H···Cl hydrogen bonds to the chloride ion. On the other hand, if the rather small water molecule, as it is the case, would be close to the NH^+ group it can easily enter the rather crowded (by other atoms) environment around the protonated lidocaine ion and thus form two strong NH^+···O hydrogen bonds and leave on its other side enough room for the chloride ion to form O–H···Cl^- hydrogen bonds.

Thus there is more stabilizing hydrogen bonding possible with the water molecule next to the NH^+ group and the chloride ion approaching the hydrogen atoms in the water molecule from the other side of the oxygen atom as the optimization shows in Fig. 1. This argument is supported by the appearance of the broad 2500 cm^{-1} band only in the infrared spectrum of the hydrated salt (Fig. 2) and not in the IR spectrum of lidocaine [14], which must be a result of N–H^+···O hydrogen bonding [19].

4.2. Vibrational spectra and assignments

The vibrational wavenumbers of the protonated lidocaine (ammonium cation) which is used as a model of the lidocaine·HCl·H_2O salt were calculated at the B3LYP/6-311G** level of calculation (Table S6) and compared to the observed ones in the infrared and Raman spectra of the lidocaine hydrochloride monohydrate (Table 4). Normal coordinate calculations of the protonated lidocaine were carried out to provide reasonable vibrational assignments of the normal vibrational modes of the lidocaine salt. The protonated lidocaine has C_1 symmetry and its 114 vibrational modes span the A irreducible representation. The lidocaine·HCl·H_2O salt has 126 vibrational modes and all span the A irreducible representation. Complete assignments of the normal modes of the cation were proposed on the basis of normal coordinate calculations, calculated infrared band intensities, Raman line activities and depolarization ratios. The vibrational modes associated with the HCl and H_2O Moieties were assigned using the GaussView program [24]. The vibrational assignments of lidocaine·HCl·H_2O are listed in Tables 4 and S6. The following discussion will be focused only on the assignments of the intense spectral lines that characterize the lidocaine salt.

The NH and CH stretching vibrations are observed as distinct, broad and moderately intense bands above the 2900 cm^{-1} spectral region of the infrared spectrum of the lidocaine·HCl·H_2O salt (Fig. 2). In comparison, the N-H stretching mode (100% PED) in the infrared spectrum of the neutral lidocaine was assigned to the observed band at 3252 cm^{-1} [14]. In the lidocaine salt this mode is assigned to the observed band at 3189 cm^{-1} (Fig. 2). This leaves the observed doublet at 3452 and 3414 cm^{-1} in the infrared spectrum of the hydrated salt to be the NH^+ stretching mode (100% PED). The splitting and the broadness of this band support the presence of moderate hydrogen bonding in the lidocaine salt as reported by the X-ray study where the molecules are determined to be linked in chains with H-bonding [30,31]. The next lower intense mode is observed at 2979 cm^{-1} in the Raman spectrum of the cation and it is calculated to be associated with the methylene group symmetric stretching (88% S_{61}). At 2948 cm^{-1} there is a very intense line also in the Raman spectrum, which is calculated to be 79% methylene antisymmetric stretching in the ethyl subgroup A (S_{79}). The next strong line at 2924 cm^{-1} is again in the Raman spectrum of the salt and is mixed from 53% methylene symmetric stretching and 34% methyl antisymmetric stretching in the ethyl subgroup B (S_{89}). All other CH stretching modes are observed with weak or medium intensities (Table 4).

In the Raman spectrum of the parent compound lidocaine one very strong line at 2922 cm^{-1} appears which is composed of methyl and methylene (smaller contribution) CH stretches in the ethyl subgroups A and B [14], while in the salt due to structural changes in those ethyl groups the methylene stretches are shifted and also splitted to two strong lines at 2948 cm^{-1} and 2979 cm^{-1} (Fig. 4). On the other hand the isolated methylene and methyl stretches in the cation appear as a very strong line at 2924 cm^{-1} (Table 4), resulting in a triplet of very strong lines in the Raman spectrum of the cation, while there is only one line in this region in the parent compound spectrum, in which the isolated methylene stretch appears as a weak line at 3018 cm^{-1}. Between 2333 and 2690 cm^{-1} in the infrared spectrum of the monohydrate there are four bands of very weak and medium intensity which must be due to hydrogen bonding interactions with water. This system of bands is not present in the parent lidocaine which contains no water [14].

The C=O stretching mode is assigned to the splitted infrared band at 1676 and 1650 cm^{-1} which is calculated to have 71% PED and a small amount of mixing with HNC scissoring (13%) and methylene twisting (10%) modes. The splitting of the C=O stretching vibration supports the existing of the salt in hydrogen bonded chains [30,31]. In the infrared spectrum of the parent lidocaine this band is observed as a single very intense band at 1666 cm^{-1} [14].

In the infrared spectrum of lidocaine a very strong and broad band is observed at 1498 cm^{-1} which contains mainly methyl antisymmetric deformations and has a shoulder at 1448 cm^{-1} that is composed mainly of ring stretching deformations [14]. In the spectrum of the hydrochloride monohydrate salt, this band is observed as splitted two distinct very intense bands at 1543 cm^{-1} (HNC scissoring) and at 1475 cm^{-1} (methylene scissoring) (Fig. 2). The shift of the methyl deformations in the 1475 cm^{-1} band in the infrared spectrum of the salt as compared to the parent drug is probably due to the presence of the methyl groups close to the chloride ion and the water molecule.

Table 4
Calculated (B3LYP/6-311G**) vibrational wavenumbers (cm^{-1}) of the non-planar form of lidocaine hydrochloride monohydrate.

Observed[a,b]		Calculated	Obs/Calc	Assignment[c]
Infrared	Raman			
3452 (w)		3580	0.96	100% NH^+ str (S_{70})
3414 (w)				
3189 (w)		3437	0.93	100% amide-NH str (S_{32})
	3067 (sh)	3171	0.97	89% CH_2 as str (S_{65})
3044 (w)	3042 (m)	3158	0.96	63% CH_2 as str in C_2H_5 (B) (S_{107})
				26% CH_3 as str in C_2H_5 (B) (S_{101})
3011 (w)	3010 (sh)	3148	0.96	62% CH_2 as str in C_2H_5 (A) (S_{89})
				23% CH_3 as str in C_2H_5 (A) (S_{83})
	2979 (vs)	3096	0.96	88% CH_2 s str (S_{61})
2951 (w)	2948 (vs)	3087	0.95	79% CH_2 s str in C_2H_5 (A) (S_{79})
2917 (w)	2924 (vs)	3077	0.95	53% CH_2 s str in C_2H_5 (B) (S_{97})
				34% CH_3 as str in C_2H_5 (B) (S_{89})
2917 (w)		3062	0.95	78% CH_3 (A) as str (S_{44})
	2894 (sh)	3056	0.95	75% CH_3 s str C_2H_5 (B) (S_{100})
2854 (vw)		3041	0.94	86% CH_3 s str in C_2H_5 (A) (S_{82})
		3026		100% CH_3 (B) s str (S_{52})
2647 (w)				$NH^+\cdots OH_2$ (hydrogen bond)
2607 (w)				
2548 (w)				
2481 (w)				
1676 (vs)	1658 (w)	1770	0.95	71% C=O str (S_{33})
1650 (vs)				13% HNC scissor (S_{36})
				10% CH_2 twist (S_{66})
1597 (vw)		1636	0.98	54% ring str def I (S_8)
				23% HNC scissor (S_{36})
				18% m-CH ipl bend (S_{25})
				17 % p-CH ipl bend (S_{27})
	1573 (w)	1632	0.96	55% ring str def I (S_8)
				13% HNC scissor (S_{36})
				11% m-CH ipl bend (S_{25})
1543 (s)	1542 (m)	1530	1.01	57% HNC scissor (S_{36})
				13% ring str def I (S_8)
				12% m-CH ipl bend (S_{25})
				10% p-CH ipl bend (S_{27})
1475 (s)		1477	1.00	50% CH_2 scissor (S_{62})
				22% CH_3 s def in C_2H_5 (A) (S_{85})
				22% CH_3 s def in C_2H_5 (B) (S_{103})
	1457 (vs)	1457	1.00	35% m-CH ipl bend (S_{26})
				21% CH_3(A) s def (S_{46})
				23% CH_3(B) s def (S_{52})
				14% ring str def I (S_8)
1439 (m)	1431 (s)	1436	1.00	43% NC_2H rock (S_{75})
				33% CH_3 rock in C_2H_5 (B) (S_{87})
				20% CH_2 twist in C_2H_5 (B) (S_{109})
1395 (m)	1388 (s)	1394	1.00	50% CH_2 rock (S_{67})
				20% CH_2 rock in C_2H_5 (A) (S_{92})
				20% CH_2 rock in C_2H_5 (B) (S_{110})
				10% HNC scissor (S_{36})
1373 (m)		1376	1.00	33% CH_2 twist (S_{66})
				27% CH_2 twist in C_2H_5 (A)(S_{91})
				25% CH_2 twist in C_2H_5 (B)(S_{109})
1317 (w)	1319 (m)	1322	1.00	43% m-CH ipl bend (S_{25})
				42% p-CH ipl bend (S_{27})
				11% ring str def III (S_{10})
	1296 (sh)	1308	0.99	21% CH_2 twist (S_{66})
				20% CH_2 twist in C_2H_5 (A) (S_{91})
				20% CH_2 twist in C_2H_5 (B) (S_{109})
				19% HNC scissor (S_{36})
1275 (m)	1272 (vs)	1283	0.99	23% ring breathing (S_7)
				19% o-CC s str (S_1)
				11% m-CH ipl bend (S_{25})
				11% p-CH ipl bend (S_{27})
1247 (w)	1236 (w)	1235	1.01	63% CH_2 twist (S_{68})
				21% HNC scissor (S_{36})
				10% ring str def III (S_{10})
1197 (w)	1194 (w)	1199	1.00	34% m-CH ipl bend (S_{23})
				33% p-CH ipl bend (S_{27})
1171 (vw)	1172 (sh)	1185	0.99	33% ring str def II (S_9)
				25% m-CH ipl bend (S_{25})
				23% ring-N str (S_3)
				10% CC str in C_2H_5 (B) (S_{108})
1151 (w)	1156 (m)	1163	0.99	26% CH_3 as def in C_2H_5 (A) (S_{86})
				14% CH_2 wag in C_2H_5 (A) (S_{81})
1127 (vw)	1125 (w)	1126	1.00	29% CH_3 as def in C_2H_5 (A) (S_{86})
				17% CH_2 wag in C_2H_5 (A) (S_{81})

(*continued on next page*)

Table 4 (*continued*)

Observed[a,b]		Calculated	Obs/Calc	Assignment[c]
Infrared	Raman			
1093 (vw)	1094 (s)	1115	0.98	39% ring str def IV (S_{11}) 38% m-CH ipl bend (S_{25}) 11% ring-N str (S_3)
1063 (vw)	1065 (sh)	1065	1.00	48% CH_3 rock in C_2H_5 (A)(S_{87}) 45% CH_3 rock in C_2H_5 (B) (S_{105})
1037 (m)	1044 (s)	1055	0.98	42% CH_3(A) rock (S_{50}) 47% CH_3(B) rock (S_{57})
987 (w)	992 (m)	987	1.00	21% CH_2 wag (S_{63})
955 (w)	959 (m)	942	1.01	33% C_8C_{10} wag (S_{38}) 11% CH_3 as def in C_2H_5 (A) (S_{86}) 11% CH_3 as def in C_2H_5 (B) (S_{104}) 11% NCO scissor (S_{41}) 10% CH_2 twist in C_2H_5 (A) (S_{91}) 10% CH_2 twist in C_2H_5 (B) (S_{109})
917 (vw)	921 (w)	917	1.00	85% m-CH wag (S_{29})
881 (w)	895 (w)	893	0.99	63% NC_2H as str (S_{72}) 12% CH_3 rock in C_2H_5 (A) (S_{87}) 13% CH_3 rock in C_2H_5 (B) (S_{105})
851 (vw)	854 (w)	854	1.00	40% ring str def V (S_{12}) 21% m-CH ipl bend (S_{26}) 19% ring-N str (S_3) 18% NC_2H as str (S_{72})
808 (w)	812 (w)	811	1.00	56% CH_2 wag in C_2H_5 (A) (S_{81}) 41% CH_3 as def in C_2H_5 (A) (S_{86})
788 (vvs)	786 (w)	703	0.99	47% m-CH wag (S_{30}) 46% p-CH wag (S_{28})
	752 (w)	757	0.99	37% NC_2H s str str (S_{71}) 39% ring str def III (S_{10})
718 (w)	726 (w)	731	0.98	25% NC_2H s str (S_{71}) 23% NCO scissor (S_{41}) 22% m-CH wag (S_{29}) 20% ring tors def I (S_{18})
688 (vw)	693 (m)	692	0.99	27% ring str def I (S_8) 25% ring-N str (S_3) 21% o-CC s str (S_1) 11% NC_2H s str (S_{71})
666 (vw)	665 (m)	625	1.06	70% NCO def (S_{41}) 13% CH_2 wag (S_{63}) 11%HNC twist (S_{40})
596 (m)	610 (w)	*604*	0.99	H_2O deformation
554 (vw)	560 (w)	548	1.01	71% HNC twisting def (S_{40}) 13% CH_2 wag (S_{63}) 12% NC_2H rock (S_{75})
528 (w)	518 (w)	524	1.01	48% HNC twisting def (S_{40}) 13% ring tors def II (S_{19}) 11% o-CC wag (S_{11}) 10% CH_3(A) rock (S_{48}) 10% CH_3(B) rock (S_{57})
482 (vw)	482 (w)	505	0.95	29% HNC twist (S_{40}) 27% m-CH wag (S_{29}) 27% p-CH wag (S_{28})
454 (w)	463 (m)	471	0.96	37% o-CC bend (S_4) 35% HNC twist (S_{40})
420 (w)	418 (w)	420	1.00	37% NC_2H s def (S_{71}) 21% CH_2 wag (S_{63}) 19% CH_2 wag in C_2H_5 (A) (S_{81}) 17% CH_2 wag in C_2H_5 (B) (S_{99})
	382 (sh)	388	0.98	25% NC_2H s def (S_{73}) 24% CH_2 wag (S_{63}) 19% CH_2 wag in C_2H_5 (A) (S_{81}) 19% CH_2 wag in C_2H_5 (B) (S_{99})
	359 (vw)	356	1.01	61% o-CC bend (S_4) 23% CH_2 wag (S_{63}) 11% HNC wag (S_{39})
	337 (vw)	337	1.00	61% HNC wag (S_{39}) 21% o-CC bend (S_4) 11% CH_2 wag (S_{63})
	316 (vw)	319	0.99	40% o-CC wag (S_{16}) 19% p-CH wag (S_{28}) 15% HNC scissor (S_{36})
	242 (s)	249	0.97	82% CH_3 torsion in C_2H_5 (B) (S_{113})

[a] Intensity abbreviations: vw: very weak, w: weak, m: medium, s: strong, vs: very strong, vvs: very very strong.

[b] *Abbreviations:* s: symmetric, as: antisymmetric, str: stretch, tors: torsional, def: deformation.

[c] CH_3(A) denotes the methyl group bound to carbon C_7 and CH_3(B) the methyl group bound to carbon C_3, while C_2H_5(A) denotes ethyl group A containing the carbon atom C_{14}, and C_2H_5(B) contains the carbon atom C_{13}. Italic denotes a calculated wavenumber for the lidocaine·HCl·H_2O.

A strong Raman line is observed at 1457 wavenumbers that is calculated to be highly mixed and consisting mostly of methyl deformations in both the ethyl groups and of m-CH in plane bend. At 1431 and 1388 cm^{-1} appear two further strong Raman lines, which are mainly consisting of rocking deformations of the methyl and methylene groups in the two ethyl subunits, of methylene rocking, and of the rocking deformation of the NC_2H^+ group (Table 4). At 1272 cm^{-1} a very strong Raman line is seen which is predicted to be highly mixed and to have 23% ring breathing. The next lower features in both spectra are of weak or at most of medium intensity (Fig. 2). The strong intensity Raman lines observed at 1094 and 1044 cm^{-1} are composed of ring stretching deformation, m-CH in plane bending, and rocking deformations of the two methyl groups at the ring (Table 4). The next lower strong spectral feature is observed in the infrared spectrum at 788 cm^{-1} and consists of m-CH (47%) and p-CH (46%) wagging vibrations. Then follows at lower wavenumbers, again a series of weak, very weak, or medium intensity spectral features.

In the Raman spectrum of the neutral lidocaine in the region around 600–700 cm^{-1} there are two remarkable very strong lines, one at 708 cm^{-1}, consisting of HNC wagging and HNC twisting, another is at 619 cm^{-1}, consisting of NCO wagging and ring-N in plane bending [14]. In the Raman spectrum of the monohydrate salt most lines are very weak or weak, medium at most, with the lines containing NCO scissoring, ring torsional deformation or even deformation of the hydrate water (Fig. 2). The HNC twisting mode can be found at 560 cm^{-1} (71% PED) with weak intensity and the HNC wagging is at 337 cm^{-1} (61% PED) with even very weak intensity in the Raman spectrum of the salt (Table 4). The ring-N in plane bend cannot be seen at all in the monohydrate Raman spectrum.

The medium intensity band at 596 cm^{-1} in the infrared spectrum of the hydrochloride monohydrate is composed of H_2O deformation and naturally not present in the neutral compound. In the infrared spectrum of the parent compound there is a strong band at 598 cm^{-1} which is composed of mainly ring deformations [14]. The very weak shoulder in the Raman spectrum of the hydrochloride monohydrate at 382 cm^{-1} is composed mainly of NC_2H symmetric deformation and methylene wagging deformations. In the same spectrum at 542 cm^{-1} of the parent compound there is a medium band composed of ring deformations [14]. At 528 cm^{-1} in the hydrated salt there is a weak band in the infrared spectrum which is composed mainly of HNC twisting deformation (Table 4). A weak band in the parent at 523 cm^{-1} is again ring deformation [14]. Thus there are three distinct bands in the spectrum of the parent compound, but only a medium one together with a weak and very weak one in the spectrum of the hydrate. The presence of the water molecule and the chloride ion changes the geometry and therefore the observed and calculated line intensities and positions.

In this region also the last strong line at 489 wavenumbers appears in the infrared spectrum of the parent which is composed of ring bending deformation and NCO rocking deformation [14]. In the infrared spectrum of the hydrated salt there is no more strong intensity band down to 420 wavenumbers, where the last weak band is seen in the infrared spectrum. The lowest line in the Raman spectrum of the salt is observed at 242 cm^{-1} with strong intensity. It is calculated to have 82% methyl torsions in the two ethyl subgroups.

4.3. ^1H and ^{13}C NMR spectral assignments

The spectral assignments were made based on substituent effects and multiplicity. The experimental chemical shifts were compared to the DFT calculated ones in Table 3. On comparison, the calculated and observed chemical shifts of lidocaine·HCl·H_2O are in excellent agreement (Table 3). The root mean square deviation (RMSD) between experiment and theory for the H atoms chemical shifts is calculated to be 2.32 ppm (Table 3). The RMSD for the C atoms chemical shifts is calculated to be 8.21 ppm. The largest experimental-calculated difference in the chemical shift (δ) is about 9.76 ppm for carbon atom C3 of the benzene ring. For the methyl carbon atoms (C18 and C21) attached to the aromatic ring, the difference is about 2 and 4 ppm. For the methylene (C13 and C14) and methyl carbons (C15 and C16) of the N-ethyl moiety the difference is found to be in the range 2–5 ppm (Table 3).

The ^1H NMR spectrum of anhydrous lidocaine hydrochloride matches with its hydrate except that the latter has the water signal appearing at a chemical shift (δ) of 2.06 ppm. Usually, a water signal is known to be concentration dependent, however, for the current hydrate the position of the signal remained the same at various concentrations of the salt in deuterochloroform. The protons (H28–H33) of the two methyl groups in $N(CH_2CH_3)_2$ appeared as a six-proton triplet at δ 1.50 ppm. It is interesting to note that the CH_2 protons in $N(CH_2CH_3)_2$ (H24–27) become magnetically nonequivalent as a result of the presence of the chiral center at the protonated N(12); the diasterotopic protons (H24 and H25 or H26 and H27) appeared as separate signals at δ 3.40 ppm as a doublet of quartet of doublet (dqd) and at δ 3.54 ppm as a quartet of doublet (qd). The splitting pattern in dqd suggests the participation of the N(12)–H(40) bond coupling as also confirmed by the splitting of neighboring protons (H22, H23) into a doublet at δ 4.42 ppm (Fig. 3). The H11 and H40 are exchangeable protons; in the ^1H NMR spectrum, taken after the sample was treated with D_2O, revealed the absences of the corresponding signals at δ 10.18 and 11.07 ppm, respectively. The singlet signal at δ 2.25 is attributed to the two CH_3 protons marked H34 to 39. While aromatic proton H17 appeared at δ 7.06 ppm, aromatic protons marked H19 and H20 had absorptions at δ 7.02 ppm. Restricted rotation around the crowded C(2)–N(1) bond makes H19 and H20 somewhat different as suggested by the splitting of the neighboring H17 as a doublet of doublet instead of a triplet. For the H atoms chemical shifts, the largest experimental-calculated difference of δ 6.36 ppm for H43 of H_2O is understandable since the locations of hydroxyl protons are difficult to predict.

Lidocaine hydrochloride monohydrate has nine different carbon signals as expected. The signal at δ 164.15 is assigned to the carbonyl signals (C8). The aromatic carbons marked C2–7 appeared in the range δ 127.48 to 135.11 ppm. The NMR signals of C10, 13, 15, and 18 are displayed at δ 50.94, 49.13, 10.00, and 18.69 ppm, respectively (Fig. 4).

On comparison with the neutral lidocaine, the effect of the difference between the neutral nitrogen in lidocaine and its protonated form in lodicaine·HCl·H_2O salt is expected to cause differences in the chemical shifts of the magnetic nuclei in the vicinity of the nitrogen centers. As such, the ^1H spectrum reveals that the protons (Hs) marked 22/23, 24/25 and 28/29/30 of lidocaine·HCl·H_2O (Fig. 3) are shifted downfield (i.e. to higher values of chemical shifts δ) compared to the corresponding protons of lidocaine (Fig. 3). The downfield shifts are due to the greater electronegativity of NH^+ compared to N; the inductive withdrawal of the σ-electrons reduces the negative charge densities of the Hs. The magnitude of the decrease in the charge density and the chemical shifts is the most for the nearest neighbors. The situation for the ^{13}C chemical shifts, however, is somewhat complex. The protonation also leads to the change in ^{13}C chemical shifts $\Delta\delta_C$ (i.e. $\delta_{C\ \text{protonated form}} - \delta_{C\ \text{free base}}$), that has been defined as a shift induced by protonation [32,33]. The definition assumes that the protonated forms exhibit no stereochemical change with respect to the free base. However, since there are some changes in the stereochemistry, $\Delta\delta_C$ may be considered as the combined effects of both protonation and geometry change. Contrary to the changes in proton chemical shifts, protonation causes upfield shifts for most of the ^{13}C signals [33].

The cause of upfield shifts has been explained by theoretical study for some amines [33]. While the electron charge densities of all of the hydrogen atoms decrease upon protonation, the charge densities of all of the carbon atoms increase. The results of the study suggest that the protonation induced upfield ^{13}C shift is attributed to the increase in the total negative charge densities on the carbon due to the C–H bond polarization (C^{-}---H^{+}) with respect to the free amine. The experimental $\Delta\delta_C$ for the C(8), C(10) and C (15/16), all in the vicinity of NH^{+}, were determined to be −7.29, −6.6 and −2.60, respectively, while for the C(13/14) the $\Delta\delta_C$ did not follow the trend, it was found to have a positive value of +0.65. To our delight, the calculated $\Delta\delta_C$ value for the C(8) also predicted an upfield chemical shift of −4.17 with respect to the free amine lidocaine. Note that the magnitude of protonation induced upfield shift is in line with the alternation effect ($\Delta\delta_C$ N–C_α < $\Delta\delta_C$ N–C_β) as predicted by Pople and co-authors [34].

5. Conclusion

Lidocaine hydrochloride monohydrate is predicted at the B3LYP/6-311G** level of theory to exist predominantly in a *gauche* structure with a NCCN torsional angle of 110° at ambient temperature. Reliable vibrational assignments of the normal modes of the lidocaine salt in its low energy *gauche* structure were provided on the basis of normal coordinate calculations and combined theoretical and experimental data. The analysis of the observed vibrational spectra is consistent with the presence of lidocaine·HCl·H_2O in one predominant conformation at room temperature. The RMSD between experimental and theoretical ^{1}H and ^{13}C chemical shifts is estimated to be 2.32 and 8.21 ppm, respectively.

Acknowledgement

The authors gratefully acknowledge the support of this work by King Fahd University of Petroleum and Minerals.

Appendix A. Supplementary data

Supplementary data associated with this article can be found, in the online version, at http://dx.doi.org/10.1016/j.saa.2015.07.060.

References

[1] J.R. Mao, L.L. Chen, Pain 87 (2000) 7–17.
[2] Y. Xia, E. Chen, D.L. Tibbits, T.E. Reilley, T.D. McSweeney, J. Clin. Anesth. 14 (2002) 339–343.
[3] N.B. Finnerup, F. Biering-Sorensen, I.L. Johannesen, A.J. Terkelsen, G.I. Juhl, A.D. Kristensen, S.H. Sindrup, F.W. Bach, T.S. Hensen, Anesthesiology 102 (2005) 1023–1030.
[4] O.A. De Leon-Casasola, J. Pain Symptom Manage. 33 (2007) 356–364.
[5] I.R. Wilhelm, A. Tzabazis, R. Likar, R. Sittl, N. Griessinger, Eur. J. Anesthesiol. 27 (2010) 169–173.
[6] C.E. Argoff, Mayo Clin. Proc. 88 (2013) 195–205.
[7] J. Sawynok, Eur. J. Pain 18 (2014) 465–481.
[8] S. Khot, C.L. Morgan, S. Kadambande, C.D. Poole, Curr. Med. Res. Opin. 30 (2014) 1573–1578.
[9] T. Narahashi, D.T. Frazier, Neurosci. Res. 4 (1971) 65–99.
[10] G.R. Strichartz, J. Gen. Physiol. 62 (1973) 37–57.
[11] B.P. Bean, C.J. Cohen, R.W. Tsien, J. Gen. Physiol. 81 (1983) 613–642.
[12] K.S. Lee, J.R. Hume, W. Giles, A.M. Brown, Nature 291 (1981) 325–327.
[13] B.R. Fink, A.M. Cairns, Anesthesiology 60 (1984) 111–120.
[14] H.M. Badawi, W. Forner, S.A. Ali, Spectrochim. Acta Part A 142 (2015) 382–391.
[15] M. Bambagiotti-Alberti, B. Bruni, M. Di Vaira, Acta Crystallogr. E 63 (2007) O768–O770.
[16] M.F. Sheets, H.A. Fozzard, G.M. Lipkind, D.A. Hanck, Trends Cardiovasc. Med. 20 (2010) 16–21.
[17] H.A. Fozzard, M.F. Sheets, D.A. Hanck, Front Pharmacol. 2 (68) (2011) 1–6.
[18] M.M. Mcnulty, G.B. Edgerton, R.D. Shah, D.A. Hanck, H.A. Fozzard, G.M. Lipkind, J. Physiol. (Lond) 581 (2007) 741–755.
[19] G.A. Neville, Z.R. Regnier, Can. J. Chem. 47 (1969) 4229–4235.
[20] M. J. Frisch, G. W. Trucks, H. B. Schlegel, G. E. Scuseria, M. A. Robb, J. R. Cheeseman, G. Scalmani, V. Barone, B. Mennucci, G. A. Petersson, H. Nakatsuji, M. Caricato, X. Li, H. P. Hratchian, A. F. Izmaylov, J. Bloino, G. Zheng, J. L. Sonnenberg, M. Hada, M. Ehara, K. Toyota, R. Fukuda, J. Hasegawa, M. Ishida, T. Nakajima, Y. Honda, O. Kitao, H. Nakai, T. Vreven, J. A. Montgomery, Jr., J. E. Peralta, F. Ogliaro, M. Bearpark, J. J. Heyd, E. Brothers, K. N. Kudin, V. N. Staroverov, T. Keith, R. Kobayashi, J. Normand, K. Raghavachari, A. Rendell, J. C. Burant, S. S. Iyengar, J. Tomasi, M. Cossi, N. Rega, J. M. Millam, M. Klene, J. E. Knox, J. B. Cross, V. Bakken, C. Adamo, J. Jaramillo, R. Gomperts, R. E. Stratmann, O. Yazyev, A. J. Austin, R. Cammi, C. Pomelli, J. W. Ochterski, R. L. Martin, K. Morokuma, V. G. Zakrzewski, G. A. Voth, P. Salvador, J. J. Dannenberg, S. Dapprich, A. D. Daniels, O. Farkas, J. B. Foresman, J. V. Ortiz, J. Cioslowski, and D. J. Fox, Gaussian, Inc., Wallingford CT, 2010.
[21] R. Ditchfield, J. Chem. Phys. 56 (1972) 5688–5692.
[22] K. Wolinski, J.F. Hilton, P. Pulay, J. Am. Chem. Soc. 112 (1990) 8251–8260.
[23] W. Forner, H.M. Badawi, J. Mol. Model. 7 (2001) 288–305.
[24] GaussView, Version 5.0, R. Dennington II, T. Keith, J. Millam, Semichem Inc., Shawnee Mission, KS, 2009.
[25] M. Shukr, Arch. Pharm. Res. 37 (2014) 882–889.
[26] C. Moch, D. Salmon, L.R. Armesto, M. Colombel, C. Pivot, F. Pirot, Int. J. Phram. 464 (2014) 91–103.
[27] M. Preis, C. Woertz, K. Schneider, J. Kukawka, J. Broscheit, N. Roewer, J. Breitkreutz, Eur. J. Pharm. Biopharm. 86 (2014) 552–561.
[28] A. Swiety-Pospiech, Z. Wojnarowska, J. Pionteck, S. Pawlus, A. Grzybowski, S. Hensel-Bielowka, K. Grzybowska, A. Szulc, M. Paluch, J. Chem. Phys. 141 (2014) 079901.
[29] G. Bhatia, A.K. Banga, Biomed. Res. Int. (2014) 537941.
[30] A.W. Hanson, M. Roehrl, Acta Crystallogr. B28 (1972) 3567–3571.
[31] H. Hamaed, J.M. Pawlowski, B.F.T. Cooper, R. Fu, S.H. Eichhorn, R.W. Schurko, J. Am. Chem. Soc. 130 (2008) 11056–11065.
[32] I. Morishima, K. Yoshikawa, K. Okada, T. Yonezawa, K. Goto, J. Am. Chem. Soc. 95 (1973) 165–171.
[33] J.E. Sarneski, H.L. Surprenant, F.K. Molen, C.N. Reilley, Anal. Chem. 47 (1975) 2116–2124.
[34] J.A. Pople, M.S. Gordon, J. Am. Chem. Soc. 89 (1967) 4253–4261.